Ab Initio Molecular Dynamics Simulation of the Aqueous Ru^{2+}/Ru^{3+} Redox Reaction: The Marcus Perspective†

Jochen Blumberger and Michiel Sprik*

Department of Chemistry, University of Cambridge, Cambridge CB2 1EW, United Kingdom

Received: September 29, 2004; In Final Form: November 21, 2004

A well-behaved (low spin) transition metal aqua ion, Ru_{aq}^{2+}, is used as a model system in an ab initio molecular dynamics study of a redox half reaction to which the Marcus theory of electron transfer is assumed to apply. Using constraint methods, we show that aqueous Ru^{2+} can be reversibly transformed to Ru^{3+} under the control of the classical solvent electrostatic potential as order parameter. The mean force is found to vary linearly with the order parameter in accordance with the Marcus theory. As can be expected for a half reaction, the slope in the oxidized and reduced states are asymmetric differing by approximately a factor of two. As a further test, we verify that the corresponding quadratic potential of mean force is in excellent agreement with the free energy profile obtained from the Gaussian distribution of potential fluctuations sampled from free (unconstrained) runs of the reduced and oxidized system. Similar to experimental electrochemical methods, our simulation scheme enables us to manipulate the effective thermodynamic driving force and align the free energy minima of product and reactant state. The activation energy and reaction entropy computed under these conditions are discussed and analyzed from the Marcus perspective.

1. Introduction

The theoretical work of Marcus on electron-transfer allowed experimentalists to interpret and understand their experiments and even make predictions based on existing data.[1−5] Marcus theory has also guided and motivated the computational study of electron transfer. On the basis of classical transition state theory, Marcus theory provided an ideal framework for Molecular Dynamics (MD) simulation of electron transfer in solution.[6−20] The objective of most studies was to validate the assumptions and implications of Marcus theory using atomistic model Hamiltonians. As an example we mention the work of Chandler and co-workers on the aqueous $Fe^{*2+} + Fe^{3+} \rightarrow Fe^{*3+} + Fe^{2+}$ self-exchange reaction.[9] It was found that the representation of diabatic free energy surfaces in terms of a quadratic dependence on the solvent electrostatic potential, a key approximation in Marcus theory, is indeed justified for this reaction (or to be more precise, for the simple point charge force field used to describe the system).

In the present paper, we show how such a Marcus inspired investigation can be generalized to density functional theory (DFT) based ab initio MD("Car-Parrinello").[21] We will make use of a grand canonical extension of this method which we have recently developed for the calculation of redox potentials.[22−24] Our method deviates from most classical simulations of electron transfer in at least one important aspect, apart from the use of electronic structure calculation. The majority of classical studies focuses on the transfer of an electron from a donor species D to an acceptor A

$$D + A = D^+ + A^- \tag{1}$$

Reaction eq 1 is indeed the original model reaction in Marcus theory and a natural starting point for the study of the kinetics of electron transfer. In contrast, the elementary process simulated in our approach is a half reaction

$$R \rightarrow O + e^- \tag{2}$$

where O and R in eq 2 now indicate the oxidized and reduced species. Model systems contain only a single redox active ion solvated by explicit solvent molecules. The aqua ion (or rather the entire solution) is either in the O(xidized) or R(educed) state. To switch oxidation state the system must find a surface crossing between the potential energy surface (PES) of the O and R state. Hopping between surfaces changes the (integer) number of electrons and the method can be formally derived from the grand canonical partition function of the electronic system in the limit of zero temperature.[22] This is the reason that we often refer to our approach as the Grand Canonical Molecular Dynamics (GCMD) method. On the other hand, the same scheme can also be compared to the multiple surface methods used for the simulation of adiabatic nonradiative transitions between excited states and ground states and is, seen from this angle, perfectly in line with the Marcus picture of electron transfer. In fact, the GCMD method can be considered as a direct application of the Marcus theory of heterogeneous electron transfer.[4,5] This connection, which we failed to recognize in our earlier publications,[22−24] is rather illuminating and will be made more explicit in the present paper. It is also the point of view adopted by a classical simulation of a heterogeneous electron transfer that has recently come to our attention, namely the computational study of an electrode process in ref 16.

The reasons for preferring half reactions over full redox reactions are in part related to a variety of technical complications introduced by the density functional electronic structure calculation (more details will be given in section 2). However, the change of perspective also opens up new opportunities for manipulating the system. Similar to the electrochemist who can

* To whom correspondence should be addressed. E-mail: ms284@cam.ac.uk.

† Part of the special issue "David Chandler Festschrift".

10.1021/jp0455879 CCC: $30.25
Published on Web 01/22/2005

control the thermodynamic driving force by applying a voltage to the electrodes of an electrochemical cell, we are now able to vary the difference in free energy between oxidation states in a computation without changing the chemical nature of the reaction. This is achieved by shifting the PES of the oxidized state with respect to the PES of R by a constant bias μ. Moreover, by a proper choice of μ it is possible to align the free energy minima of the reduced and oxidized states. At this point, the O and R species are in a 1:1 thermodynamic equilibrium and the corresponding value $\mu = \mu_{1/2}$ can be used as an estimate of the free energy of oxidation[22] (see also section 2.4).

This procedure of counterbalancing the thermodynamic driving force by lowering or raising the PES of one of the oxidation states was applied in a study of $Ag^{+}_{aq} \rightarrow Ag^{2+}_{aq} + e^{-}$ and $Cu^{+}_{aq} \rightarrow Cu^{2+}_{aq} + e^{-}$ half reactions in ref 23. As the duration of our MD runs is too short to establish true equilibrium between species, the value of $\mu_{1/2}$ was estimated from the irreversible transition in oxidation state in an upward and downward sweep of μ. Subtracting the free energies of the two half reactions obtained in this way gave a redox potential for the full reaction in good agreement with experiment. The result for the $Ag^{+}_{aq} \rightarrow Ag^{2+}_{aq} + e^{-}$ oxidation was validated in an independent calculation using an alternative implementation of the GCMD method.[24] The value of μ was fixed at the estimate of $\mu_{1/2}$ obtained in ref 23 and the system was carried over from the reduced to the oxidized state by a controlled variation of the coordination number of the ion.

One of the observations made during the simulation of the Ag^{+} and Cu^{+} redox reactions is that the solvent reorganization accompanying the oxidation is rather severe. This is consistent with the d^{10} coordination chemistry of these ions and is the reason that we were able to use the coordination number as an order parameter. As a result, these reactions cannot be classified as outershell and are therefore less suitable for an analysis of simulation results in the light of Marcus theory. On the other hand the $Fe^{2+}_{aq} \rightarrow Fe^{3+}_{aq} + e^{-}$ reaction which has played such a dominant role in the theoretical investigations of electron transfer is not a very convenient model system for ab initio MD because of the high spin character of the coordination complex. This led us to the "equivalent" reaction involving Ruthenium cations

$$Ru^{2+}_{aq} \rightarrow Ru^{3+}_{aq} + e^{-} \tag{3}$$

Similar to the Fe aqua-ions, Ru is in both oxidation states coordinated by 6 water molecules in more or less octahedral symmetry. The major difference between the two octahedra is the Ru−O distance which is 0.08 Å[25] smaller in the oxidized state. However, while the oxidation states of Ru ions have the same *d* electron configuration as the Fe ion, they are low spin. Moreover, both complexes are stable in aqueous solution and have been investigated for more than fifty years by optical[26−29] and electrochemical measurements.[26,28,30] Compounds of Ru^{2+} and Ru^{3+} have also been popular in the experimental literature on electron-transfer reactions.[25,30,31]

This paper is organized as follows: We start in section 2 with an outline of the relevant theory highlighting the distinction between adiabatic and diabatic free energies which links our method to the Marcus theory of homogeneous electron transfer and the electrochemist's view of heterogeneous electron transfer. The grand canonical simulation methods introduced in refs 22 and 24 are briefly reviewed from this new perspective. In section 2, we also define the electrostatic potential as order parameter used for reaction eq 3. The implementation of the constrained molecular dynamics scheme is described in section 3. More technical details concerning the molecular dynamics and electronic structure methods are given in the appendix. The free energy and energy profiles obtained for reaction eq 3 are discussed in section 4 and validated by the results obtained from equilibrium simulations of reactant and product. Entropic contributions are compared to experimental results and discussed. The results of this work are summarized and concluded in section 5.

2. Theory

2.1. Marcus Theory. In his treatment of homogeneous electron exchange (eq 1) Marcus introduced two intersecting diabatic free energy surfaces, one for the reactant state $R = D + A$ and one for the product state $P = D^{+} + A^{-}$. These free energy surfaces are assumed to be quadratic in an appropriate reaction coordinate x.

$$G_M(x) = G_M^* + \frac{k}{2}(x - x_M)^2 \; M = \mathrm{R, P} \tag{4}$$

where x_R and x_P are the equilibrium values of the reaction coordinate in reactant, respectively, product state and G^*_R and G^*_P, the values of the corresponding equilibrium free energies. k is a spring constant assumed to be the same for reactant and product state. The central quantity in Marcus theory derived from the diabatic free energy profiles is the reorganization free energy. It is defined for reactant and product states as

$$\lambda_P = G_P(x_R) - G_P(x_P) \tag{5}$$

$$\lambda_R = G_R(x_P) - G_R(x_R) \tag{6}$$

λ_R and λ_P are in general different. However, adopting the quadratic approximation of eq 4 with equal curvature in product and reactant surfaces these quantities reduce to

$$\lambda = \frac{k}{2}(x_P - x_R)^2 \tag{7}$$

The activation free energy for the forward reaction can be expressed in terms of the reorganization free energy leading to the famous Marcus gap law

$$\Delta G^{\ddagger} = \frac{(\lambda + \Delta G)^2}{4\lambda} \tag{8}$$

with the thermodynamic driving force given by

$$\Delta G = G^*_P - G^*_R \tag{9}$$

2.2. Energy Surfaces. Simulation attempts to arrive at these results by postulating a set of diabatic potential energy surfaces and determining the free energy profile for variation of the reaction coordinate x by averaging over all other microscopic degrees of freedom for a given energy surface. The question is then how to construct a suitable set of diabatic PESs. This is relatively easy when a classical point charge model is used. If q_A and q_D are the charges on the acceptor and donor ions in the reactant state, then the corresponding PES can be expressed as

$$V_R(\mathbf{R}^N) = \frac{q_A q_D}{R_{12}} + \sum_{I=3}^{N}\left[\frac{q_A q_I}{R_{1I}} + \frac{q_D q_I}{R_{2I}}\right] + \frac{1}{2}\sum_{I,J=3}^{N}\frac{q_I q_J}{R_{IJ}} + V_{\mathrm{pair}}(\mathbf{R}^N) \tag{10}$$

where R_{IJ} is the distance between atoms I and J with point charges q_I and q_J, respectively. For convenience, the donor ion has been labeled as $I = 1$ and the acceptor ion as $I = 2$. So, $q_1 = q_D$ and $q_2 = q_A$. Index values $I = 3,...,N$ label interaction sites of solvent molecules. V_{pair} stands for some short-range pair potential complementing the model. The (diabatic) PES of the product state is obtained by replacing the charges of donor and acceptor ions with their values after electron exchange according to eq 1.

$$V_P(\mathbf{R}^N) = \frac{(q_A - 1)(q_D + 1)}{R_{12}} + \sum_{I=3}^{N}\left[\frac{(q_A - 1)q_I}{R_{1I}} + \frac{(q_D + 1)q_I}{R_{2I}}\right] + \frac{1}{2}\sum_{I,J=3}^{N}\frac{q_I q_J}{R_{IJ}} + V_{pair}(\mathbf{R}^N) \quad (11)$$

The adiabatic PES is constructed from the diabatic PESs of eqs 10 and 11 according to

$$V(\mathbf{R}^N) = \min[V_R(\mathbf{R}^N), V_P(\mathbf{R}^N)] \quad (12)$$

The simple point charge model potentials of eqs 10 and 11 have been the basis for most of the classical simulation studies. In practice, of course, the parametrization of a realistic force field can be a major task, in particular in the case of transition metal ion complexes. This problem is eliminated in ab initio MD but replaced by a complication of a more fundamental nature: The unstable branch of a diabatic surface requires the determination of an electronic excitation energy (including its gradient). Unfortunately, excited state techniques are generally less accurate and more costly compared to ground state methods. Moreover, even the ground state calculation is not completely reliable at the level of the GGA approximation to DFT used in ab initio MD methods because of the tendency to charge delocalization which could lead to spurious fractional charges on the ions.

These DFT related problems were at the root of our decision to abandon full reactions (eq 1) as model systems and use half reactions (eq 2) instead. The excited states are replaced by ionization states which can be treated as groundstates. Thus, if we write for the PES of the reduced state

$$E_R(\mathbf{R}^N) = E_{N_e}^{(0)}(\mathbf{R}^N) \quad (13)$$

where $E_{N_e}^{(0)}(\mathbf{R}^N)$ is the ground state of an N_e electron system, the PES of the oxidized system becomes the groundstate of a system with one electron less

$$E_O(\mathbf{R}^N) = E_{N_e-1}^{(0)}(\mathbf{R}^N) \quad (14)$$

The PESs of eqs 13 and 14 should be compared to the classical diabatic surfaces of eqs 10 and 11. Similar to eq 12 these energy surfaces are combined to an effective adiabatic ionic potential, however including a constant shift applied to the O surface

$$E_\mu(\mathbf{R}^N) = \min[E_R(\mathbf{R}^N), E_O(\mathbf{R}^N) + \mu] \quad (15)$$

The forces on the ions, i.e., derivatives of E_μ wrt ion coordinates, depend on the choice of the parameter μ: If $-\mu$ is smaller than the instantaneous (vertical) ionization potential

$$\Delta E_{vt}(\mathbf{R}^N) = E_O(\mathbf{R}^N) - E_R(\mathbf{R}^N) \quad (16)$$

the forces are determined by the PES of R and by the PES of O otherwise.

2.3. Heterogeneous Electron Transfer and Electrochemistry. Equation 15 was derived in ref 22 by taking the zero temperature limit of the adiabatic electronic grand potential restricted to two states R and O. In this grand canonical view, the constant μ can be identified with the chemical potential of a fictitious reservoir of electrons which has no interaction with the system other than exchange of electrons. The reservoir therefore acts as an idealized electrode. This parallel can be made more explicit by considering the electron exchange as heterogeneous electron transfer between an ion and a metal surface. Here, we enter the realm of electrochemistry and electrochemists have developed a variety of models of increasing sophistication to understand this process. The model that is relevant for us is the most elementary picture of an outershell process leading to oxidation. The ion in the reduced state R is assumed to release its electron when it arrives in the outer Helmholtz plane, which is some distance away from the metal surface. Interaction with the surface is minimal and the hydration shell essentially remains intact. In a heterogeneous system such as an electrochemical cell, the average (macroscopic) electrostatic potential is an important quantity because it is in general not the same in the two phases. Denoting the potential in the electrolyte by ϕ_s and in the metal by ϕ_m, the difference $\phi_s - \phi_m$ can be interpreted as the finite potential step across the bilayer forming the interface. The electron transfer can be decomposed into two steps: transfer of the electron from the ion (ϕ_s) to vacuum ($\phi = 0$) and from vacuum to the electrode (ϕ_m). The first step requires an energy input equal to the ionization potential $e\phi_s$ (e is the elementary charge) which is added to the PES of R to obtain the PES of O. The energy gained in the second step should be added to the PES of O (product) amounting in first approximation to a shift of the PES of O relative to the PES of R by $-e\phi_m$.

This argument found in most electrochemistry textbooks (see, e.g., ref 32) is very appealing. It offers a direct and intuitive route to eq 15 establishing a relation between the constant μ and the electrode potential ϕ_m. Also our scheme of varying μ, thereby shifting the PES of the oxidation states with respect to each other, is supported by this interpretation: It mimics the controlled changes of ϕ_m achieved in experiment by connecting the metal to an external potential source. Finally, this simple picture of an electrode process provides the foundation of the application of Marcus theory to heterogeneous electron transfer and by implication to the redox half reaction eq 2. All expressions in Section 2.1 remain valid with the reduced state R functioning as reactant R and the oxidized state O as product P.

2.4. Diabatic Free Energies. The central quantities in Marcus theory are the two energies appearing in the gap law eq 8, namely the thermodynamic driving force ΔG and the reorganization free energy λ. Simulation methods intended to test Marcus theory should be capable to deliver both energies. To determine the reaction free energy we must be able to distinguish reactant from product. In general, this requires the specification of an order parameter, which can be a difficult problem (see below). When, however, a set of diabatic surfaces is available, as is the case for model electron-transfer reactions, introduction of order parameters can be avoided.[23] The free energy of oxidation (eq 2)

$$\Delta A = A_O - A_R \quad (17)$$

is directly obtained from separate configurational integrals over

the diabatic energy surfaces E_R and E_O of eq 13 and 14

$$A_M = -k_B T \ln \Lambda^{-3N} \int d\mathbf{R}^N \exp[-\beta E_M(\mathbf{R}^N)] \quad (18)$$

The symbols in eq 18 have the usual meaning: $\beta = 1/(k_B T)$ with T the ionic temperature and k_B the Boltzmann constant. Λ is the average thermal wavelength defined as $\Lambda^{-3N} = \Pi_j \lambda_j^{-3N_j}/N_j!$ with λ_j the thermal wavelengths $\lambda_j = h/\sqrt{2\pi m_j k_B T}$ of the nuclei species j and N the total number of nuclei. Substituting the vertical ionization potential ΔE_{vt} of eq 16 we can rewrite the diabatic oxidation free energy eq 17 in a form familiar from umbrella sampling methods

$$\Delta A = -k_B T \ln \langle \exp(-\beta \Delta E_{vt}) \rangle_R \quad (19)$$

$$= k_B T \ln \langle \exp(\beta \Delta E_{vt}) \rangle_O \quad (20)$$

with $\langle \cdots \rangle_M$ denoting the configurational average on the PES E_M. Under exceptional conditions, which are in fact fulfilled for reaction 3 (see below), eqs 19 and 20 can be used to compute the redox free energy. Normally, however, some form of stepwise reversible transformation between oxidation states is needed. The transformation used in the numerical titration scheme introduced in ref 22 exploits the freedom of choice for the parameter μ in eq 15. The method searches for the particular value $\mu = \mu_{1/2}$ for which the system has equal probability to be in the O and R state (in practice the middle of a hysteresis loop consisting of an upward and downward sweep of μ). It can be shown that under these conditions of 1:1 equilibrium

$$\Delta A = -\mu_{1/2} \quad (21)$$

with ΔA the oxidation free energy of eq 17. A proof of eq 21 is given in ref 22. The method was applied in ref 23 to estimate the free energies of the redox couples Ag^+/Ag^{2+} and Cu^+/Cu^{2+}. We note that a similar order parameter free diabatic approach can be applied to homogeneous electron transfer (eq 1) using the classical PESs of eqs 10 and 11.

If it is our goal to compare to Marcus theory (eq 4) an order parameter is clearly essential. Marcus suggested to use the solvent electrostatic potential acting on the ions. The potential at the site of an ion can be expressed in the notation introduced in section 2.2 as

$$\phi(\mathbf{R}^N) = \phi_1(\mathbf{R}^N) = \frac{1}{\phi_0} \sum_n \sum_{I=2}^{N} \frac{q_I}{|\mathbf{R}_I + \mathbf{n}L - \mathbf{R}_1|} \quad (22)$$

where the redoxactive ion is labeled 1 and H and O atoms from 2 to N. Since it is convenient to deal with order parameters without physical dimension (so the corresponding mean force is an energy) $\phi(\mathbf{R}^N)$ has been normalized by a potential constant ϕ_0 such that the numerical value of the potential is effectively expressed in Volt (see appendix). In simulation of liquids the atoms are usually contained in a (small) periodic simple cubic unit cell with length L. The summation of lattice vectors $\mathbf{n}L$ for calculation of long-range interactions, which was suppressed in eqs 10 and 11, has now been explicitly included. The appropriate reaction coordinate for homogeneous electron transfer (eq 1) is the difference $\phi(\mathbf{R}^N) = \phi_1(\mathbf{R}^N) - \phi_2(\mathbf{R}^N)$ where 1 and 2 label donor and acceptor atoms. In case of redox half reactions, we can directly use the ion potential $\phi(\mathbf{R}^N) = \phi_1(\mathbf{R}^N)$ which is also in line with the parallel to heterogeneous electron transfer discussed in section 2.3.

How to evaluate a Marcus-type order parameter in ab initio MD simulation? The problem confronting us in electronic structure calculation is that the electrostatic potential exhibits a highly structured spatial dependence reflecting atomic, molecular and intermolecular features. Most of this information is not needed in the Marcus order parameter complicating its interpretation and making it impossible to use this quantity as a mechanical constraint. We avoided this problem by simply using a classical solvent potential. The DFT charge distribution is replaced by classical point charges on the O and H atoms for which we used the SPC values for liquid water. The order parameter is then computed again according to eq 22 substituting the atomic positions generated by the ab initio MD.

The statistics of the order parameter of eq 22 is contained in the probability distribution

$$p_M(\phi') = \frac{\int d\mathbf{R}^N \exp[-\beta E_M(\mathbf{R}^N)] \delta(\phi(\mathbf{R}^N) - \phi')}{\int d\mathbf{R}^N \exp[-\beta E_M(\mathbf{R}^N)]} \quad (23)$$

or, alternatively, in the corresponding Landau free energy profile

$$W_M(\phi') = -k_B T \ln \Lambda^{-3N} \int d\mathbf{R}^N \exp[-\beta E_M(\mathbf{R}^N)] \delta(\phi(\mathbf{R}^N) - \phi') = -k_B T \ln p_M(\phi') + A_M \quad (24)$$

where A_M is the diabatic free energy of eq 18. The expression for the free energy of eq 24 is completely general and the extent to which it fits a quadratic dependence on ϕ' is a direct test of the assumptions in Marcus theory(see section 3.1 and ref 9).

For a computation of the reorganization energies of eqs 5 and 6 we must be able to distinguish between the nonequilibrium free energy after vertical excitation (ionization) and the free energy of the relaxed equilibrium state. Following the textbook of Chandler,[33] we assume that for stable reactant and product species the fluctuations of the order parameter are confined to well-defined basins, described by the intervals $\Phi_R = [\phi_{R1}, \phi_{R2}]$ for the reactant and $\Phi_P = [\phi_{P1}, \phi_{P2}]$, for the product. Φ_R and Φ_P are centered around the average values ϕ_R and ϕ_P, respectively. The free energy corresponding to this definition of equilibrium states $M = R, P$ is the integral

$$A_M^h = -k_B T \ln \Lambda^{-3N} \int d\mathbf{R}^N h_M(\mathbf{R}^N) \exp[-\beta U_M(\mathbf{R}^N)] \quad (25)$$

h_M is 1 if $\phi(\mathbf{R}^N) \in \Phi_M$ and 0 otherwise. U_M is again a diabatic PES as in eq 18. So, $U_M = V_M$ (eqs 10 and 11) for homogeneous electron transfer ($R = D + A$, $P = D^+ + A^-$) or E_M (eqs 13 and 14) for heterogeneous electron transfer (R=R, P=O). The free energies of eq 25 differ from those defined in eq 18 by the restriction of the full configurational integral to the equilibrium basins h_M. They can be obtained from the Landau free energy $W_M(\phi')$ of eq 24 by integration over the order parameter interval Φ_M

$$A_M^h = -k_B T \ln \int_{\Phi_M} d\phi' \exp[-\beta W_M(\phi')] = A_M - k_B T \ln \int_{\Phi_M} d\phi' p_M(\phi') \quad (26)$$

We see that $A_M^h \geq A_M$, in accordance with the minimal properties of the exact free energy. The correction term $A_M^h - A_M$ tends to zero when the interval Φ_M is extended over the entire range of values for the order parameter ϕ.

The reorganization free energy can now be written as a similar diabatic free energy integral but confined to the stability basin of the other oxidation state. Thus, the expression for free energy of relaxation after vertical oxidation (λ_P in eq 5 with P = O) becomes

$$\lambda_O = -k_B T \ln \Lambda^{-3N} \int d\mathbf{R}^N h_R(\mathbf{R}^N) \exp[-\beta E_O(\mathbf{R}^N)] - A_O^h \quad (27)$$

with the integral for A_O^h given in eq 25. Reducing the configurational integral again to an order parameter integral in the style of eq 26 we find

$$\lambda_O = -k_B T \ln \int_{\Phi_R} d\phi' p_O(\phi') \quad (28)$$

where we have omitted a supposedly small $A_O - A_O^h$ correction term. Similarly the free energy associated with reorganization on the reduced PES can expressed as

$$\lambda_R = -k_B T \ln \Lambda^{-3N} \int d\mathbf{R}^N h_O(\mathbf{R}^N) \exp[-\beta E_R(\mathbf{R}^N)] - A_R{}^h = -k_B T \ln \int_{\Phi_O} d\phi' p_R(\phi') \quad (29)$$

2.5. Adiabatic Free Energies. For the argument in section 2.4 it is not necessary that ϕ is a good ("faithful") order parameter discriminating between reactant and product, which would mean that the intervals Φ_R and Φ_P are not allowed to overlap. Indeed, because of the excited state nature of some charge transfer states, it may not always be possible to find such an order parameter (the Marcus inverted region is an example of such a situation). Of course, if we want to use this variable to drive the reaction, then it is crucial that it distinguishes clearly between reactant and product state. This is the normal function of order parameters. Such an enforced conversion (or the construction of an underlying transition path ensemble) takes place on an adiabatic PES U_{ad} (V of eq 12 or E_μ of eq 15) generating a corresponding adiabatic free energy

$$A_M{}^{ad} = -k_B T \ln \Lambda^{-3N} \int d\mathbf{R}^N h_M(\mathbf{R}^N) \exp[-\beta U_{ad}(\mathbf{R}^N)] \quad (30)$$

For homogeneous electron transfer the distinction between the diabatic free energy of eq 25 and the adiabatic counterpart of eq 30 (and by implication ΔA) is negligible, provided reactant and product state can be separated, i.e., R and P PES cross *between* the equilibrium intervals Φ_R and Φ_P. In that case, both yield the same estimate of the reaction free energy, so $\Delta A_{ad} = \Delta A^h$ where $\Delta A_{ad} = A^{ad}{}_P - A^{ad}{}_R$ and similarly for ΔA^h.

The situation is more complicated for heterogeneous electron transfer on which we focus for the remainder of this paper. The difference wrt homogeneous electron transfer is that the surface crossing point depends on the vertical shift parameter μ. To make this dependence explicit, we change to a notation specific for half reactions and replace the superscript ad in eq 30 by the subscript μ. By varying μ we can adjust the location where the reaction occurs as already discussed in the context of the numerical titration method (eq 21). Substituting eq 15 into eq 30 we see that the simple linear relationship between diabatic and adiabatic PES is carried over to the free energy[24]

$$\Delta A^h = -\mu + \Delta A_\mu \quad (31)$$

Equation 31 is only valid for a finite range of values of μ with upper and lower limits imposed by the conditions for the existence of two minima on the adiabatic PES. Beyond these critical values of μ, the reaction can no longer proceed by a radiationless transition (but may still be induced by photoionization).

Equation 31 can be regarded as a computational chemistry modification of the Nernst equation

$$\Delta_r G^\ominus = -F\epsilon + \Delta G \quad (32)$$

In eq 32, $\Delta_r G^\ominus = -F\epsilon^\ominus$ is the standard reaction free enthalpy of oxidation, ϵ^Q the standard electrode potential defined for the oxidation half reaction eq 2, F the Faraday constant, ϵ the electrode potential and $\Delta G = -k_B T \ln(a_O/a_R)$ the concentration dependent free enthalpy term where a_M denotes the activity of M, M = R,O. If in the limit of infinite dilution ΔA^h equals the standard free enthalpy difference between O and R, μ/F can be interpreted as the electrode potential ϵ and the adiabatic free energy difference ΔA_μ identified with ΔG (the difference between enthalpies and energies is not relevant here). For redox reactions between solvated ions, the detailed nature of the metal electrode is irrelevant which explains why our method can disregard it (see also ref 34).

To estimate ΔA_μ the adiabatic PES E_μ connecting product and reactant states is sampled by constraint methods or by umbrella sampling techniques at a suitable fixed value of μ producing the adiabatic free energy profile

$$W_\mu(\phi') = -k_B T \ln \Lambda^{-3N} \int d\mathbf{R}^N \exp[-\beta E_\mu(\mathbf{R}^N)] \delta(\phi(\mathbf{R}^N) - \phi') \quad (33)$$

The corresponding reaction free energy is given by

$$\Delta A_\mu = -k_B T \ln \frac{\int_{\Phi_P} d\phi' \exp[-\beta W_\mu(\phi')]}{\int_{\Phi_R} d\phi' \exp[-\beta W_\mu(\phi')]} \quad (34)$$

Details for the computation of $W_\mu(\phi')$ from constrained molecular dynamics simulation are given in the appendix.

3. Molecular Dynamics Method

3.1. Gaussian Model and Free Energy Computation. Two series of molecular dynamics simulations of the ruthenium ion oxidation reaction in water (eq 3) have been carried out: One set of runs consists of free (unconstrained) dynamics on the diabatic energy surfaces E_R and E_O of eqs 13 and 14. The second set are constrained trajectories on the adiabatic surface E_μ of eq 15 for fixed values of the electrostatic order parameter ϕ of eq 22.

These runs serve two main purposes. A first objective is to examine whether our Ru^{2+}/Ru^{3+} model system complies to the Marcus theory. A first indication can be obtained by comparing the equilibrium order parameter distributions eq 23 obtained from the (free) diabatic simulations to a Gaussian

$$p_M(\phi') = \frac{1}{\sqrt{2\pi}\sigma_M} \exp\left[-\frac{(\phi' - \phi_M)^2}{2\sigma_M{}^2}\right] \quad (35)$$

If the fluctuations can be described by this function, then the Landau free energy derived according to eq 24 has a quadratic dependence on ϕ'

$$W_M(\phi') = W_M^* + \frac{k_B T}{2\sigma_M{}^2}(\phi' - \phi_M)^2 \quad (36)$$

which is of the same parabolic form as eq 4. The inverse square width

$$\left.\frac{d^2 W_M}{d\phi'^2}\right|_{\phi'=\phi_M} = \frac{k_B T}{\sigma_M{}^2} \equiv k_M \quad (37)$$

plays the role of the linear (mean) force constant entering the Marcus expression for reorganization free energy (eq 7), where we now have allowed for a different curvature for reduced and oxidized free energy surface.

The data produced by the adiabatic constrained MD runs can be used for a independent verification of adherence to Marcus theory. The requirement now is that the mean force varies linearly with the value of the constraint on the order parameter (classical electrostatic potential). More specifically, this means that the conditional averaged gradients (see eq 48 of the appendix) can be written as

$$\left\langle \frac{\partial \mathrm{H}_\mu}{\partial \phi} \right\rangle_{\phi'}^{\text{cond.}} = k_M(\phi' - \phi_M) \tag{38}$$

where ϕ_M is the nearest equilibrium value. We have carried out constrained runs on the composite surface eq 15 for a given value μ (see below). The more direct approach would have been to use constrained trajectories on the separate component diabatic surfaces E_O and E_R. However, we have chosen the adiabatic approach as it allows for the computation of the diabatic free energy profiles up to the crossing point and simultaneously for the computation of the reaction free energy (see below). We want to emphasize that the two branches of the profiles corresponding to E_μ are truly diabatic because the switch between PESs E_O and E_R only occurs at the crossing point of the profiles but not in the equilibrium regions. In principle, the diabatic profiles could be extended to the excited-state region by replacing the adiabatic PES E_μ with the corresponding diabatic PES. Of course, the continuation of runs would have increased the accuracy of the linear fit, but we have left it out due to computational cost. Ideally, the coefficients k_M in eqs 37 and 38 should be identical. Discrepancies between these two quantities are therefore a quantitative measure of the accuracy of our sampling techniques. The final check of how well either of the computed free energy surfaces are described by a quadratic function is to use the force constants to determine the reorganization energies eq 7, substitute these values in the gap law eq 8 and compare the free energy barrier obtained this way to the free energy where our system is observed to change oxidation state in the simulation. A second objective of our two-track simulation approach is a critical investigation of the thermochemistry. Again, data from the free and constrained schemes will be compared and tested for consistency. The basis for the determination of the redox free energy ΔA from unconstrained simulations is the relation to $\mu_{1/2}$ of eq 21. As explained in ref 23, the procedure for estimating $\mu_{1/2}$ consists of sliding the PES for the oxidized state past the PES for the reduced state by varying μ in an upward and downward sweep. The result are two S-shaped curves for the (average) number of electrons in the system. The curves are displaced with respect to each other by hysteresis effects. $\mu_{1/2}$ is equated with the value of μ at midpoint of the hysteresis loop. This "titration" scheme, applied in ref 23, is expensive requiring a sequence of adiabatic simulations, each run adding to the computational cost. However, for well-behaved redox systems, which can be described by two intersecting parabolic free energy surfaces (Marcus regime), it is possible to obtain a reliable estimate of $\mu_{1/2}$ from eqs 19 and 20 requiring just two regular diabatic runs (i.e., $\mu = 0$), one on the oxidized PES and one on the reduced PES. As will be demonstrated in a forthcoming publication,[35] the redox free energy under these conditions is to very good approximation given by the mean of the average vertical ionization potential ΔE_{vt} of the oxidized and reduced species.

$$\Delta A = -\mu_{1/2} \approx \frac{1}{2}\left(\langle \Delta E_{vt}\rangle_R + \langle \Delta E_{vt}\rangle_O\right) \tag{39}$$

where the subscripted brackets denote averages over an equilibrium trajectory in oxidation state $M = R, O$. Application to the diabatic runs of Ru^{2+} and Ru^{3+} aqua ions studied here yields $\mu_{1/2} = 0.58$ eV.

The strategy for testing this result against an independent estimate of redox free energy obtained from a simulation on the connected adiabatic surface E_μ of eq 15 makes use of the observation that for the specific choice of $\mu = \mu_{1/2}$ the corresponding free energy profile W_μ of eq 33 has the structure of a double well potential with almost degenerate minima (the minima are exactly degenerate if the curvature of oxidized and reduced branch is the same, see eq 42). The formalism of sections 2.4 and 2.5 enables us to be precise and make the conditions for turning this observation into a method for the computation of free energy more explicit. An absolutely crucial requirement is that ϕ' is a good order parameter capable of distinguishing between product and reactant species. This implies that the stability intervals Φ_O and Φ_R must be well separated and can be extended far enough such that the correction term in eq 26 can be neglected without risking overlap between Φ_O and Φ_R. In that case, we can replace A_M in eq 21 by ΔA^h. Substituting in eq 31 we can make a series of identifications leading to the conclusion that ΔA_μ vanishes if all the assumptions we have made are justified.

$$\Delta A_\mu = \Delta A^h + \mu_{1/2} \approx \Delta A + \mu_{1/2} = 0 \tag{40}$$

Finally, we must relate ΔA_μ to the change in Landau free energy $W_\mu(\phi')$ of eq 33, because this is the quantity that is computed as the reversible work needed to transform reactant into product. What is involved in making this last step, is best seen in the framework of the Marcus theory. So, expanding W_μ with respect to its two minima at ϕ_O and ϕ_R to second order in the order parameter we can substitute eq 37 for the second derivative and obtain

$$W_\mu(\phi') = W_\mu(\phi_M) + \frac{k_B T}{\sigma_M^2}(\phi' - \phi_M)^2 + ... \tag{41}$$

Inserting in eq 34 gives

$$\Delta A_\mu = W_\mu(\phi_O) - W_\mu(\phi_R) - k_B T \ln\frac{\sigma_O}{\sigma_R} + ... \tag{42}$$

The width σ_M of the fluctuations of ϕ' in the two oxidation states, while not identical, are sufficiently similar for the contribution to rhs of eq 42 to be small (see further section 4.1). Taken together eqs 40 and 42 imply that the consistency of our grand canonical method demands that for a μ fixed at $\mu_{1/2}$ the mean force on the constrained electrostatic field driving the reaction should integrate to a net reversible work of zero. A similar calculation was carried out in ref 24 for the Ag^+/Ag^{2+} oxidation using coordination number as order parameter.

3.2. Technical Implementation. The practical implementation of the MD simulation experiment outlined in the previous section requires a suitable assignment of a number of technical parameters. We need to decide on the range of values of the order parameters to be investigated. The equilibrium values of ϕ in the reduced and oxidized state were found to be $\phi_R = -6.91$ and $\phi_O = -8.68$ (see section 4.1). Constrained CPMD runs were carried out for eight values of ϕ equidistantly distributed over this interval. One series of runs was performed

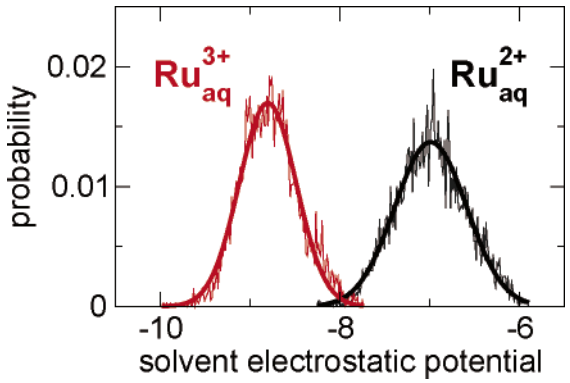

Figure 1. Distribution of the electrostatic solvent potential ϕ on the metal site (classical Marcus order parameter) for Ru^{2+} (black) and Ru^{3+} (red) ions obtained from equilibrium (diabatic) simulations of one ion in 32 water molecules at 300 K. ϕ, defined in eq 22, was evaluated by Ewald summation (eq 52) using the SPC charges for O and H atoms ($q_O = -2q_H = -0.8476e$). Computed distributions (thin lines) are fitted to Gaussians (thick lines). The average and mean square deviation of ϕ are -6.98 ± 0.40 for Ru^{2+} and -8.78 ± 0.32 for Ru^{3+}.

from ϕ_R to ϕ_O and another series from ϕ_O to ϕ_R. For each simulation run, the first 1−2 ps of dynamics were discarded and a trajectory of variable length (2−10 ps) taken for the calculation of average Lagrange multiplier and potential energy E_μ. The initial configuration of a simulation at electrostatic potential ϕ_i was taken from an equilibrium configuration of the previous run at a potential value ϕ_{i-1}.

For simulations at a constraint value close to surface crossing the wave function was quenched to the Born−Oppenheimer (BO) surface yielding instantaneous energies for the oxidized and reduced states. The effective potential E_μ was then calculated according to eq 15 and the ionic forces determined for the next 10 CPMD steps according to eqs 49−51. The number of CPMD steps between two energy comparisons of R and O was increased up to 500 for runs close to the equilibrium values ϕ_R and ϕ_O. Further details of the MD methodology and density functional electronic structure method is given in the appendix.

A brief remark about size effects. As no explicit counterion is included in our model system, charge neutrality is imposed by the periodic boundary conditions in the form of a homogeneous distribution of negative charge. The effect of the long range interaction of the cation with its periodic images and compensating background is huge (for numbers, see ref 23). As a result only differences of oxidation energies have physical meaning and then only for redox reactions with equivalent ions on both sides of the reaction such as is the case for the $Ag^{2+} + Cu^{+} \rightarrow Ag^{+} + Cu^{2+}$ redox couple studied in ref 23. These effects are however of secondary concern in the present work, which studies a system for which the reaction free energy is made to vanish by a special choice of the potential bias ("fictitious electrode potential") μ. Note also that relaxation occurs on one and the same diabatic surface at fixed total charge. λ_O and λ_R are therefore independent of μ and supposedly less sensitive to periodic boundary conditions compared to the reaction free energies which do involve a change of charge.

4. Results and Discussion

4.1. Order Parameter Fluctuations. In Figure 1 we show the distribution of the solvent electrostatic potential (eq 22) obtained from a Car−Parrinello molecular dynamics (CPMD) trajectory of equilibrium Ru^{2+} and Ru^{3+} in 32 water molecules at 300 K.

The distributions obtained from 5 ps of CP dynamics are close to Gaussian distributions with correlation coefficients of 0.98

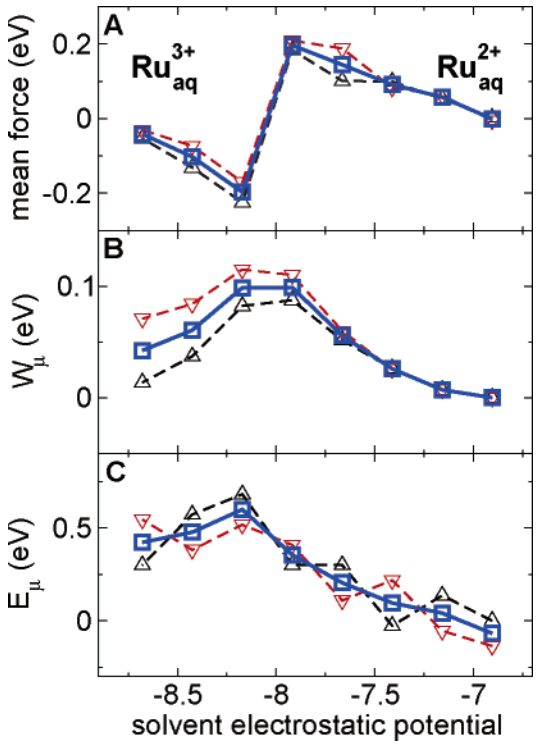

Figure 2. Mean force (A), free energy (B) and energy profile (C) for the transformation between aqueous Ru^{2+} and Ru^{3+}. The reaction coordinate is the classical solvent electrostatic potential ϕ at the metal site defined in eq 22. The oxidation half reaction is denoted by black triangles pointing upward and the reduction half reaction by red triangles pointing downward. Squares denote the average of oxidation and reduction. The mean force is approximated by the average Lagrange multiplier (eq 48) obtained from constrained grand canonical simulations on the PES E_μ (eq 15), $\mu = 0.58$ eV. Numerical integration of the mean force gives the reversible work W_μ which is set to zero for forward and back reaction at $\phi = \phi_R = -6.91$. The crossing between reduced and oxidized surface occurs between $\phi = -8.16$ and $\phi = -7.92$. The average potential energies E_μ are given using the energy at ϕ_R as reference.

and 0.97 for Ru^{2+}, respectively Ru^{3+}. The Ru^{2+} ion exhibits a broader distribution than Ru^{3+} as indicated by the larger root-mean-square deviation (width) of Ru^{2+}, $\sigma_R = 0.40$, compared to $\sigma_O = 0.32$ for Ru^{3+}.

As discussed in section 3.1 an equilibrium distribution for parameter fluctuations of the form of eq 35 was one of the criteria deciding whether our system is in the regime where Marcus theory applies. Equally important for our test is that the centers of the two distributions are separated by 1.8, i.e., by more than 4 σ_R, hence they hardly overlap. The solvent electrostatic potential ϕ at the site of the metal ion therefore indeed meets the requirements for an order parameter for the transformation between the two redox states confirming that eq 42 holds for our system. With a width ratio of $\sigma_O/\sigma_R \approx 0.8$ the contribution of the last term is negligible allowing us to use the reversible work directly as an estimate of the reaction free energy

$$\Delta A_\mu \approx W_\mu(\phi_O) - W_\mu(\phi_R) \tag{43}$$

4.2. Mean Force. In Figure 2A, the mean force approximated by the average Lagrange multiplier $\langle\lambda\rangle^t_{\phi i}$ (eq 48) is shown for the transformation between Ru^{2+} and Ru^{3+}. The root-mean-square deviations of the Lagrange multiplier are large, approximately 0.2 eV, and in the order of the average values (0−0.2 eV). The oscillations of λ around the average value are fast

on the ps time scale and do not exhibit drifts. Averaging over a trajectory of a few ps was therefore sufficient to obtain $\langle\lambda\rangle^t_{\phi i}$ to an accuracy of about 0.01 eV.

$\phi_R = -6.91$ marked the equilibrium in the reduced state and for this value of the order parameter the average Lagrange multiplier almost vanishes, $\langle\lambda\rangle^t_{\phi R} = 0.00$ eV. A decrease of the electrostatic potential constraint down to -7.92 results in a nearly linear increase of $\langle\lambda\rangle^t_{\phi i}$ to 0.18 eV (denoted by the five triangles pointing upward on the right half of Figure 2A). In this range of ϕ values, the system stays permanently in the reduced state. The constraint force of eq 53 has to pull the water molecules closer to the metal center to accommodate the more negative electrostatic potential. At $\phi = -8.16$ the water ligands are close enough to the metal center so that after a 13 fs run time, the PES of the oxidized state crosses the PES of the reduced state. From then on, the forces on the ions are derived from the PES of the oxidized state leading to rapid structural relaxation (still obeying the constraint) and separation of the potential energy surfaces by about 0.4 eV. Surface recrossing from O to R was not observed for the next ps as the thermal fluctuations were much smaller than the gap between the two surfaces. At this point, the average Lagrange multiplier changes sign and becomes negative. This is because the constraint force has to pull the water molecules now away from the metal center consistent with a more positive potential than observed for the oxidized state under equilibrium conditions. Reduction of the constraint from -8.16 to the equilibrium value of the oxidized state, $\phi_O = -8.68$, gives again a nearly linear increase of $\langle\lambda\rangle^t_{\phi i}$ from -0.22 to -0.05 eV (denoted by the three triangles pointing upward on the left half of Figure 2A).

In contrast to the oxidation of Ag^+ to Ag^{2+} (see our previous paper ref 24) the oxidation of Ru^{2+} to Ru^{3+} could be reversed to the reduced state (triangles pointing downward in Figure 2A). An increase of the constraint value from ϕ_O to -8.16 leaves the oxidation state unchanged. A further increase of ϕ to -7.92 leads to irreversible surface crossing from O to R and change of sign of the Lagrange multiplier which again nearly vanishes at ϕ_R. For all values of the constraint variable, the system stays in the same oxidation state during the forward and backward sweep. Furthermore, the mean force does not depend significantly on the direction of the reaction confirming that the solvent electrostatic potential is a suitable control variable for enforcing a reversible transformation between Ru^{2+} and Ru^{3+}. The for ab initio MD excellent reversibility gives us further confidence that the mean forces in our calculation remain well in the linear response regime in agreement with eq 38.

4.3. Redox Potential. Integration of the mean force according to eq 47 gives the free energy profile along the solvent electrostatic potential as shown in Figure 2B. The reversible work W_μ for oxidation and reduction are almost identical for constraint values that favor the reduced state ($\phi = \phi_R$ to -7.92) but differ by a few 0.01 eV in the stability interval of the oxidized state ($\phi = -8.16$ to ϕ_O). For discussion, we use the average values obtained from oxidation and reduction (denoted by squares in Figure 2). The free energy barrier is calculated to be 0.10 eV and 0.06 eV for the half reaction of oxidation and reduction, respectively, amounting to a reversible work of $\Delta W_\mu = W_\mu(\phi_O) - W_\mu(\phi_R) = 0.04$ eV for the transformation from R to O. Referring back to eqs 40 and 43, we see that this 0.04 eV of reversible work is our error margin for satisfying the consistency test for free energy computation. Translating this back into a reaction free energy we arrive at an estimate of the free energy of oxidation of $\Delta A^h \approx -\mu + \Delta W_\mu = -0.54$ eV, which should be compared to the $\Delta A = -0.58$ eV obtained from eq 39. The deviation of 0.04 eV cannot entirely be attributed to statistical errors but also reflects inaccuracies due to approximations such as the neglect of the fluctuation term in eq 42.

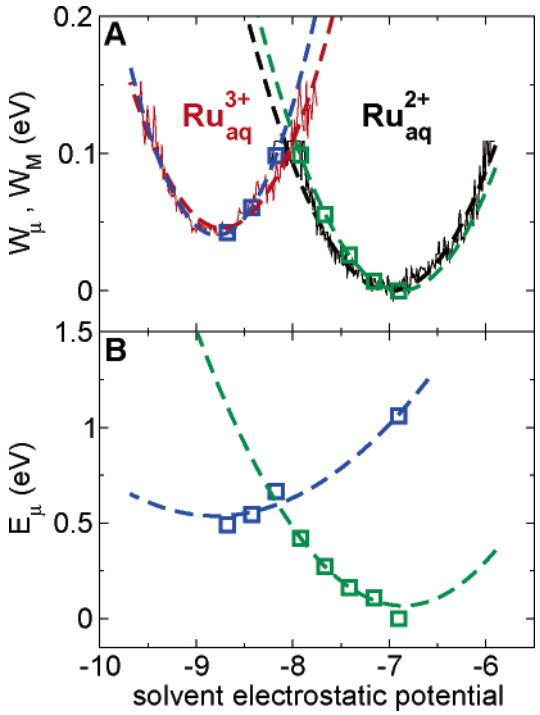

Figure 3. (A) Comparison of the free energy profiles of aqueous Ru^{2+} and Ru^{3+} obtained from equilibrium and constrained grand canonical CPMD simulations. The free energy curves W_M, M = R,O, R = Ru^{2+}_{aq}, O = Ru^{3+}_{aq}, are denoted in black and red solid lines. They are obtained from eq 24 using the equilibrium probability distributions of the solvent electrostatic potential shown in Figure 1. W_μ is denoted by squares taken from Figure 2B. Green and blue squares indicate that the system is in the oxidized respectively reduced state during the entire grand canonical simulation. Quadratic fits of W_M and of the oxidized and reduced branch of W_μ are drawn in dashed lines. (B) Quadratic fits (dashed lines) of the oxidized (blue) and reduced branch (green) of the energy profile E_μ obtained from constrained grand canonical simulations. The data points denoted by squares are taken from Figure 2(C). For the curve of Ru^{3+}_{aq} a fourth point is added at $\phi = -6.91$ as explained in the main text.

The slight overlap of the distributions of Figure 1 suggests that equilibrium simulation of one oxidation state may sample the equilibrium region of the other oxidation state sufficiently well that straightforward relative free energy computation according to eqs 19 and 20 might work. Computing the vertical ionization energies ΔE_{vt} along equilibrium trajectories of Ru^{2+}_{aq} and Ru^{3+}_{aq} and determining the exponential average we find almost identical free energies, -0.58 and -0.59 eV. This results also validates the approximate relation eq 39, which predicted a value of -0.58 eV. In conclusion, the close agreement among these numbers obtained from rather different calculation schemes supports the claim made in section 4.1 regarding the relatively small statistical errors in this simulation.

4.4. Free Energy Profile and Marcus Test. The free energy profile of Figure 2 shows a number of interesting features, such as a rather low barrier and a clear asymmetry between reduced and oxidized state. Before discussing such details we first address the crucial issue of accuracy and consistency of our results. In Figure 3 we compare the constrained free energy profile $W_\mu(\phi')$ of Figure 2 to the free energy density $W_M(\phi')$ obtained from the unconstrained runs on the PES of R and O according to eq 24. To align $W_M(\phi')$ with the two branches of

TABLE 1: Mean Values ϕ_M of the Electrostatic Order Parameter and Force Constant k_M Computed from Gaussian Fits to Two Different Free Energy Profiles[a]

	$Ru^{3+}(M = O)$		$Ru^{2+}(M = R)$	
	const.	free	const.	free
k_M	0.31 ± 0.03	0.26 ± 0.01	0.18 ± 0.04	0.15 ± 0.01
ϕ_M	-8.79 ± 0.05	-8.78 ± 0.10	-6.88 ± 0.05	-6.98 ± 0.10
λ_M	0.56 ± 0.10	0.42 ± 0.04	0.33 ± 0.04	0.24 ± 0.03
$\Delta A_M^{\ddagger}$	0.09	0.06	0.13	0.10

[a] Data obtained from fitting the reversible work function of Figure 2B are labeled *const.* and data obtained from fits to the Landau free energy associated with the equilibrium fluctuations of Figure 1 are labeled *free.* λ_M (in eV) is the corresponding reorganization free energy computed according to eq 7. $\Delta A_M^{\ddagger}$ (in eV) is the activation free energy as predicted by the Marcus gap law (eq 8) using the mean of the reorganization free energy in reduced and oxidized state and a reaction free energy for oxidation of $\Delta G = 0.04$ eV with $\Delta A_{[IMAGE]}^{\ddagger}$ and $\Delta A_{[IMAGE]}^{\ddagger}$ denoting the barrier for reduction respectively oxidation.

$W_\mu(\phi')$, $W_R(\phi')$ is defined to be zero at ϕ_R and $W_O(\phi')$ to equal the adiabatic reaction free energy density ΔW_μ at ϕ_O. As one can see in Figure 3 $W_R(\phi')$ and $W_O(\phi')$ (solid lines) match the two branches of $W_\mu(\phi')$ (squares) very well, even for order parameter values close to the crossing point. The transitions from R to O ($\phi = -8.16$) and from O to R ($\phi = -7.92$) occur for plausible values of the order parameter at which the overlap of the equilibrium distributions is maximal (Figure 1).

Next, we turn to the question whether Marcus theory applies to our system. As explained in section 3.1, a first requirement is that the free energy curves of Figure 2 are described by the parabolic dependence on order parameter of eq 36. As one can see from the quadratic fits of the two branches of $W_\mu(\phi')$ and of $W_M(\phi')$ this is a good approximation, at least for the Ru^{2+}/Ru^{3+} redox couple. The correlation coefficient for the fit of the five points of the right branch of $W_\mu(\phi')$ is 0.9997. The two profiles $W_M(\phi')$ give a somewhat lower correlation coefficient of 0.95, which is most likely due to limited sampling of order parameter values close to the crossing point.

The second derivatives obtained from the quadratic fits are listed in Table 1 together with the corresponding location of the minima. According to eq 37, the curvatures can either be interpreted as force constants k_M or as the inverse variance k_BT/σ_M^2 of the order parameter fluctuations. The table uses the force constant representation. The agreement between the results obtained from the free and constrained runs is good, with the force constants derived from the two branches of $W_\mu(\phi')$ being higher than the force constants implied by the order parameter fluctuations. This trend is brought out more clearly in the third line of the table where force constants and the values of the order parameters at the minima have been combined to reorganization free energies using eq 7. This formula can be viewed as a single point approximation to the more general expressions eqs 28 and 29 for the case of Gaussian probability densities p_M. As explained in section 3.1, we use the comparison between force constants as quantitative test of the consistency between free and constrained simulation and therefore the accuracy of our results. We find a discrepancy of approximately 20%. While the agreement could be better, we regard it as a sufficient basis to conclude that the linear response regime essentially spans the entire stability range of an oxidation state as measured by the electrostatic order parameter, which is the main condition for the validity of Marcus theory.

The final test is then to see how these data work out when substituted in the gap law. The force constants of Table 1, referring to half reactions, show a significant asymmetry. However, it can be shown that as long as the difference is not too large, eq 8 is still a good approximation for the free energy barrier if we take for λ the mean reorganization free energy $\lambda = 1/2(\lambda_O + \lambda_R)$. This is how the activation energies given in Table 1 have been computed. To be consistent with the small but finite oxidation free energy of 0.04 eV of Figure 2B we have set the thermodynamic driving force ΔG in the gap law equal to this number. The results should be compared to the activation free energies directly obtained from the data in Figure 2B without any fits. The numbers are, in the notation of Table 1, an activation free energy of $\Delta A_R^{\ddagger} = 0.1$ eV for the R $\rightarrow$ O reaction and $\Delta A_O^{\ddagger} = 0.06$ eV for the reaction in the O $\rightarrow$ R direction. Deviations between the two sets of free energy barriers are in the order of 20−30%, similar to margin between the results from constrained and free runs. We conclude therefore, that when we allow for a statistical uncertainty of this size, the results of our simulation of the $Ru^{3+} \rightarrow Ru^{2+}$ redox reaction are consistent with Marcus theory.

Summarizing the results for the free energy profile, we found that the force constant of the oxidized state is nearly a factor two larger compared to the reduced state, giving rise to a similar asymmetry in relaxation free energy. It should be pointed out, however, that the uncertainties of the values for O are significant as they were obtained by calculating the second derivative of a minimal set of three points making up the left branch of $W_\mu(\phi')$. A quantitative estimate of the asymmetry is therefore at this point still somewhat uncertain. The other feature of interest is the surprisingly low oxidation free energy barrier of 0.1 eV $= 4k_BT$. This value is small when compared to typical activation free energies for covalent bond breaking (1−2 eV) but larger than the $0.7k_BT$ estimated for the redox reaction of the Ag couple using a structural order parameter (coordination number).[24] For the transformation between Ru^{2+} and Ru^{3+} the octahedral complex does not have to undergo major structural changes but a small reduction of the Ru−O bond lengths by 0.08 Å. The activation energy required for this process may be expected to be small, possibly even as small as 0.10 eV. This suggests that it might be feasible to observe a spontaneous reaction on the 10−20 ps time scale of ab initio molecular dynamics.

4.5. Energy Profile. The energy profile for the transformation between the two redox states is shown in Figure 2(C). E_μ is estimated by the average CPMD energy obtained for the electrostatic potential constrained trajectory at 300 K. All energy values of oxidation and reduction reaction are shown relative to the average energy at the reactant equilibrium value ϕ_R. The statistical uncertainty of each point is at least 0.3 eV, which is the maximum deviation of energy between forward and backward sweep at the same value of ϕ. The convergence of the average energy value is significantly worse compared to the average Lagrange multiplier. An explanation of this effect could be that the Lagrange multiplier is a gradient of free energy measuring the local response to small changes in the order parameter, while the potential energy is an absolute quantity depending on all parts of the sample. The Lagrange multiplier was sufficiently well converged after averaging over 1−2 ps whereas the uncertainty of the potential energy is still several 0.1 eV even after averaging over up to 10ps of dynamics. For the discussion of the energy profile, we take the average energy values obtained from the oxidation and reduction reaction.

As one can see in Figure 2C the changes in energy along the reaction path are almost 1 order of magnitude larger than the variation in free energy. The activation energies for oxidation and reduction are estimated to be 0.5 respectively 0.1 eV giving a reaction energy difference $\Delta E^h \approx -\mu + \Delta E_\mu = -0.1$ eV

where $\Delta E_\mu = E_\mu(\phi_O) - E_\mu(\phi_R)$. This value should be compared to the $\Delta E = \langle E_O \rangle_O - \langle E_R \rangle_R = -0.35$ eV energy difference between average potential energy of O and R obtained from equilibrium simulations. The deviation is mainly due to the fact that the former value is an energy difference between the two CPMD-PESs of R and O whereas the latter is obtained from Born−Oppenheimer optimized energies of O and R.

As for the free energies, we have fitted the 5 points of the reduced branch of the energy profile to a harmonic function (correlation coefficient = 0.95, see Figure 3B). The relaxation energy of R, 1.2 eV, determined as the energy difference of the fit function at ϕ_O and ϕ_R, is in good agreement with the relaxation energy $\langle E_R \rangle_O - \langle E_R \rangle_R = 0.9$ eV obtained from equilibrium simulations. A harmonic fit of the three points of the oxidized branch of the energy profile gives an unrealistic high curvature. The left branch of Figure 3B is therefore extended with a fourth point at ϕ_R by adding the relaxation energy of O, $\langle E_O \rangle_R - \langle E_O \rangle_O = 0.6$ eV, to the energy at ϕ_O, $E_\mu(\phi_R) = E_\mu(\phi_O) + 0.6$ eV. According to the equilibrium simulations the relaxation energy of Ru^{2+} is 0.3 eV larger than for Ru^{3+}. This result is unexpected because it does not support the trend observed for the redox couples Ag^+/Ag^{2+}, Cu^+/Cu^{2+},[23] and RuO_4^{2-}/RuO_4^-,[35] of which the higher charged oxidation state exhibits the larger relaxation energy. It is also contrary to the behavior of the free energy profiles (section 4.4), for which O gives the steeper curve. The relaxation energy difference between O and R, 0.3 eV, is, however, almost within the error bars of the energy levels, making extrapolation very uncertain. To resolve this issue, it is clearly necessary to add more points to the oxidized curve, following the diabatic branch into the unstable region at higher values of the order parameter.

4.6. Entropy Effects. A direct comparison of the reaction free energies of section 4.3 to experiment is not possible because of the bias due to periodic boundaries. The same is true for the reaction energies of section 4.5. For analysis of entropy effects the situation is more favorable because one could argue that the huge interaction energies between periodic images and compensating background cancel to a large extent in the entropy leaving only size effects related to confinement in a too small cell (which can of course still be serious). The argument relies again on distinguishing between a diabatic ("true") reaction energy ΔE^h and a "shifted" adiabatic reaction energy ΔE_μ obtained from the constrained dynamics (Figure 2). These two energies are related by a simple linear equation

$$\Delta E^h = -\mu + \Delta E_\mu \tag{44}$$

This equation is the equivalent of eq 31 for the free energy. Substituting in the expression for the reaction entropy we find

$$\Delta S^h = \Delta S_\mu \tag{45}$$

However, for the particular choice of μ establishing a 1:1 equilibrium the thermodynamic force is zero ($\Delta A_\mu = 0$) and therefore

$$T\Delta S^h = \Delta E_\mu \tag{46}$$

Since the reaction free energy in Figure 2B indeed vanishes to a good approximation we conclude that the oxidation energy in Figure 2C can be used as a direct estimate of the reaction entropy (note the parallel to the latent heat in a phase transition). This gives $T\Delta S^h = 0.4$ eV which is close to the value of $T\Delta S = 0.2$ eV obtained from grand canonical titration. The discrepancy of 0.2 eV could again be due to the difference of the CPMD and BO estimate to ΔE as explained in the previous section.

The positive reaction entropy found for the oxidation of Ru^{2+} to Ru^{3+} is in clear disagreement with the −0.5 eV entropy difference obtained from electrochemical measurements.[36] It is also in conflict with generally held beliefs about oxidation and the models at the basis of these beliefs. Aqua-ions of high net charge are regarded as "structure making" decreasing the entropy in the solvent compared to aqua-ions of low net charge. For example, the Born relation predicts that the entropic energy of oxidation of a 2+/3+ couple is $T\Delta S = -0.609/r_B$ eV at 298 K where r_B is the effective Born radius. Taking a value of 2 Å for r_B the Born formula predicts an entropy change of approximately −0.3 eV.

The appreciable uncertainty in the mean energies is of course an important factor which could contribute to the discrepancy between calculated an experimental entropies. An observation supporting this explanation for the positive sign of the oxidation entropy is that the relaxation energy of Ru^{2+} exceeds the relaxation free energy by 0.9−0.3 = 0.6 eV. The uncertainty of the relaxation energy is, however, not expected to make up this rather large gap. On the other hand the number of water molecules used in the simulation (1 ion and 32 water molecules per cell) is almost certainly not sufficient to fully solvate the trivalent ion leading to underestimation of long range 'structure making' effects which normally take entropy out of the system.

5. Conclusion

Using a constrained ab initio MD scheme, we have shown that aqueous Ru^{2+} can be reversibly transformed to Ru^{3+} under the control of the classical solvent electrostatic potential as order parameter. The mean force is found to vary linearly with the order parameter with a discontinuity marking the reaction. This behavior is in accordance with the Marcus theory of electron transfer. The corresponding potential of mean force is found to be in excellent agreement with the free energy profile obtained from the Gaussian distribution of potential fluctuations sampled from free (unconstrained) runs of the reduced and oxidized system. The consistency between these results obtained from independent trajectories generated by different MD schemes are proof that our statistical accuracy is sufficient for a meaningful comparison to Marcus theory. The ab initio MD simulation therefore confirms the validity of Marcus theory for this model system. In view of the uncertainties usually associated with ab initio MD averages, the argument can also be turned around and the agreement with Marcus theory interpreted as evidence that our MD results are converged. The latter perspective is the more relevant in the context of a meaningful comparison to experiment.

The novel simulation scheme employed in this work enabled us to create the thermodynamic condition of a 1:1 equilibrium between oxidation states. In experimental electrochemical cells this situation can be achieved by application of a biasing external potential matching the standard potential. The computed activation free energy for the transformation of Ru^{2+} to Ru^{3+} under these conditions is found to be rather small, namely 0.1 eV which is however consistent with the value predicted by the Marcus gap law using our estimates for reorganization free energy. The free energy profiles of oxidized and reduced state show a modest asymmetry with second derivatives differing by about a factor two. Results on entropy effects remain tentative due to the large statistical uncertainties of the energy profile. They seem to indicate that the entropy of oxidation is large

and positive contributing about ~0.4 eV to the free energy. While this is the right order of magnitude, the positive sign is contrary to experimental measurements and in conflict with most theoretical models.

Considering the very limited size of the model system, describing the first coordination shell (the ligands) in full electronic detail but accounting only for a fraction of the outer solvation shell, the entropy discrepancy raises the question about the partition of free energy between inner and outer shell. This is an old issue in electrochemistry and inorganic chemistry which we hope to address in a continuation of this investigation. Another direction for further research is a careful investigation of the dependence of the activation energy and transition state on the parameter μ playing the role of cell potential in our approach. Combined with a transition state approach,[32] this could ultimately yield information that can be used to understand current−voltage relations, bringing us a step closer to application of ab initio MD methods to voltammetry.

Appendix

Molecular Dynamics Method. Aqueous solutions of Ru^{2+} and Ru^{3+} are modeled by a periodically repeated cubic cell containing one metal ion and 32 water molecules. The length of the unit cell, $L = 9.86$ Å, was chosen so that the density of water molecules was equal to the experimental density of pure liquid water at standard conditions. The ion concentration and solvent density chosen is the same used for modeling aqueous Ag^{+} [37] and Ag^{2+}.[23,24] Equilibrium and constrained grand canonical CPMD[38] simulations were carried out using a fictitious electronic mass of 500 au, a time step of 5 au (0.1209 fs) and a temperature rescaling to 300 K if the instantaneous temperature exceeded a boundary of 300 ± 50 K. Every 2000 MD steps, the wave function was optimized to the ground state and the CP dynamics restarted from the optimized wave function. Equilibrium properties of Ru^{2+} and Ru^{3+} were averaged over a trajectory of 5 ps. For the calculation of the averages eqs 19 and 20 every 50 CPMD steps the energy of oxidized and reduced state was quenched to the Born−Oppenheimer surface and the vertical ionization potential and electron affinity of the Ru^{2+} respectively Ru^{3+} solutions calculated. Details for constrained grand canonical simulation are given in the main text (section 3).

Electronic Structure Method. Pseudopotentials used for Ru, O and H were constructed according to the Troullier−Martins scheme 39. Pseudopotential parameters for O and H are given in ref 23 and for Ru in ref 40. The electron configuration [Kr] $4d^7$ of Ru^{+} is taken as a reference state and the 4*s*,4*p* and 4*d* electrons are treated as valence. The pseudization radii are 1.1 au for the *s* channel, 1.2 for *p* and 1.24 for *d*. The Kleinman−Bylander transformation was used for O and the Gauss−Hermite integration for Ru. The orbitals are expanded in plane waves with a reciprocal space cutoff of 70 Ry. The exchange-correlation energy was calculated using GGA for exchange according to Becke[41] and GGA for correlation according to Lee, Yang, and Parr.[42] The Ru pseudopotential was tested by calculating the gas-phase ionization energy of Ru^{2+}. The deviation of about 0.2 eV from the experimental value[43] was regarded as satisfactory. The aqueous solutions of Ru^{2+} (d^6) and Ru^{3+} (d^5) were simulated for the low spin configuration, $2S + 1 = 1$ and $2S + 1 = 2$, respectively. For Ru^{3+} the local spin density approximation to DFT was used.

Method of Constraints. The free energy profile $W_\mu(\phi')$ can be computed by integration over the mean force

$$W_\mu(\phi') = \int_{\phi_R}^{\phi'} d\phi'' \left\langle \frac{\partial H_\mu}{\partial \phi} \right\rangle_{\phi''}^{\text{cond.}} \tag{47}$$

where $H_\mu(\mathbf{p}^N,\mathbf{R}^N) = K(\mathbf{p}^N) + E_\mu(\mathbf{R}^N)$ denotes the Hamiltonian, E_μ the adiabatic PES defined in eq 15 and $\langle O\rangle_{\phi''}^{\text{cond.}}$ the conditional average (see ref 24 for a definition). Note that $W_\mu(\phi')$ is set equal to zero for the equilibrium value of R, $W_\mu(\phi_R) = 0$. (In ref 24 $W_\mu(\phi')$ was therefore denoted as $\Delta W_\mu(\phi')$.) The mean force is approximated by the time average of the Lagrange multiplier obtained from constrained grand canonical MD runs on the PES E_μ

$$-\left\langle \frac{\partial H_\mu}{\partial \phi} \right\rangle_{\phi''}^{\text{cond.}} \approx \langle \lambda \rangle_{\phi''}^{t} \tag{48}$$

neglecting the small correction terms derived in ref 44. The total force $\mathbf{F}_1^{\text{tot}}$ on the ion I is then given by

$$\mathbf{F}_I^{\text{tot}} = \mathbf{F}_I + \mathbf{F}_I^{\text{c}} \tag{49}$$

$$\mathbf{F}_I = -\frac{\partial E_\mu(\mathbf{R}^N)}{\partial \mathbf{R}_I} \tag{50}$$

$$\mathbf{F}_I^{\text{c}} = -\lambda \frac{\partial \phi(\mathbf{R}^N)}{\partial \mathbf{R}_I}\bigg|_{\phi''} \tag{51}$$

where $\mathbf{F}_I^c$ is the constraint force. The value of the potential constraint eq 22 at the site of the Ru atom $\mathbf{R}_1$ was calculated by Ewald summation

$$\phi(\mathbf{R}^N) = \phi_1(\mathbf{R}^N) = \frac{1}{\phi^0}\sum_{I=2}^{N} q_I \left[\sum_{\mathbf{n}} \frac{\operatorname{erfc}(\eta|\mathbf{R}_{I1\mathbf{n}}|)}{|\mathbf{R}_{I1\mathbf{n}}|} + \sum_{g\neq 0} \frac{4\pi}{V|\mathbf{g}|^2} \exp(-|\mathbf{g}|^2/(4\eta^2) + i\mathbf{g}(\mathbf{R}_I - \mathbf{R}_1)) \right] \tag{52}$$

where $\mathbf{R}_{I1\mathbf{n}} = \mathbf{R}_I + \mathbf{n}L - \mathbf{R}_1$ (in a.u.). Solvent atoms, i.e., O and H atoms, are labeled from 2 to *N*. The atomic charges were taken from the SPC model, $q_I = -0.8476e$ for oxygen and $q_I = 0.4238e$ for hydrogen atoms. $\phi(\mathbf{R}^N)$ is transformed from a.u. to Volt (V) and made dimensionless by dividing with the constant $\phi^0 = (1/27.211)$ V. The constraint force eq 51 on atom I

$$\mathbf{F}_I^{\text{c}} = -\lambda \frac{\partial \phi(\mathbf{R}^N)}{\partial \mathbf{R}_I}\bigg|_{\phi''} = \frac{1}{\phi^0}\lambda q_I \left[\sum_{\mathbf{n}} \left(\frac{2\eta}{\pi^{1/2}} \frac{\exp(-\eta^2|\mathbf{R}_{I1\mathbf{n}}|^2)}{|\mathbf{R}_{I1\mathbf{n}}|} + \frac{\operatorname{erfc}(\eta|\mathbf{R}_{I1\mathbf{n}}|)}{|\mathbf{R}_{I1\mathbf{n}}|^2} \right) \frac{\mathbf{R}_{I1\mathbf{n}}}{|\mathbf{R}_{I1\mathbf{n}}|} - \sum_{g\neq 0} \frac{4\pi}{V|\mathbf{g}|^2} \exp(-|\mathbf{g}|^2/(4\eta^2) + i\mathbf{g}(\mathbf{R}_I - \mathbf{R}_1)) i\mathbf{g} \right] \tag{53}$$

and atom 1

$$\boldsymbol{F}_1^{\,c} = -\sum_{I=2}^{N} \mathbf{F}_I^{\text{c}} \tag{54}$$

was evaluated and used to obtain the Lagrange multiplier λ applying the velocity Verlet version of the SHAKE algorithm.[45] The above expressions are similar for homogeneous electron

transfer. In this case, E_μ is replaced by the adiabatic potential of eq 12 and $\phi_1(\mathbf{R}^N)$ by $\phi_1(\mathbf{R}^N) - \phi_2(\mathbf{R}^N)$ as explained in the main text.

Acknowledgment. We thank Yoshitaka Tateyama, Ruth Lynden-Bell, and Joost VandeVondele for helpful discussion. We are particularly grateful to Joost VandeVondele for the suggestion to use a classical approximation for the electrostatic order parameter. This research was sponsored by EPSRC. J.B. is grateful to the Austrian Academy of Sciences for financial support. The bulk of the computations was carried out on the HPCx facility at Daresbury.

References and Notes

(1) Marcus, R. A. *J. Chem. Phys.* **1956**, *24*, 966.
(2) Marcus, R. A. *J. Chem. Phys.* **1956**, *24*, 979.
(3) Marcus, R. A. *J. Chem. Phys.* **1957**, *26*, 867.
(4) Marcus, R. A. *J. Chem. Phys.* **1965**, *43*, 679.
(5) Marcus, R. A. *Rev. Mod. Phys.* **1993**, *65*, 599.
(6) Warshel, A.; Hwang, J. K. *J. Chem. Phys.* **1986**, *84*, 4938.
(7) Warshel, A.; Chu, Z. T.; Parson, W. W. *Science* **1989**, *246*, 112.
(8) Hwang, J. K.; Warshel, A. *J. Am. Chem. Soc.* **1987**, *109*, 715.
(9) Kuharski, R. A.; Bader, J. S.; Chandler, D.; Sprik, M.; Klein, M. L.; Impey, R. W. *J. Chem. Phys.* **1988**, *89*, 3248.
(10) Marchi, M.; N., G. J.; Chandler, D.; Newton, M. D. *J. Am. Chem. Soc.* **1993**, *115*, 4178.
(11) Ando, K.; Kato, S. *J. Chem. Phys.* **1991**, *95*, 5966.
(12) Ando, K. *J. Chem. Phys.* **1997**, *106*, 116.
(13) Ando, K. *J. Chem. Phys.* **2001**, *114*, 9040.
(14) Ando, K. *J. Chem. Phys.* **2001**, *114*, 9470.
(15) Hartnig, C.; Koper, M. T. M. *J. Chem. Phys.* **2001**, *115*, 8540.
(16) Hartnig, C.; Koper, T. M. *J. Am. Chem. Soc.* **2003**, *125*, 9840.
(17) Straus, J. B.; Voth, G. A. *J. Phys. Chem.* **1993**, *97*, 7388.
(18) Straus, J. B.; Calhoun, A.; Voth, G. A. *J. Chem. Phys.* **1995**, *102*, 529.
(19) Calhoun, A.; Voth, G. A. *J. Phys. Chem. B* **1998**, *102*, 8563.
(20) Small, D. W.; Matyushov, D. V.; Voth, G. A. *J. Am. Chem. Soc.* **2003**, *125*, 7470.
(21) Car, R.; Parrinello, M. *Phys. Rev. Lett.* **1985**, *55*, 2471.
(22) Tavernelli, I.; Vuilleumier, R.; Sprik, M. *Phys. Rev. Lett.* **2002**, *88*, 213002.
(23) Blumberger, J.; Bernasconi, L.; Tavernelli, I.; Vuilleumier, R.; Sprik, M. *J. Am. Chem. Soc.* **2004**, *126*, 3928.
(24) Blumberger, J.; Sprik, M. *J. Phys. Chem. B* **2004**, *108*(21), 6529.
(25) Brunschwig, B. S.; Creutz, C.; McCartney, D. H.; Sham, T.-K.; Sutin, N. *Faraday Discuss. Chem. Soc.* **1982**, *74*, 113.
(26) Wehner, P.; Hindman, J. C. *J. Am. Chem. Soc.* **1950**, *72*, 3911.
(27) Cady, H. H.; Connick, R. E. *J. Am. Chem. Soc.* **1958**, *80*, 2646.
(28) Mercer, E. E.; Buckley, R. R. *Inorg. Chem.* **1965**, *4*, 1692.
(29) Harzion, Z.; Navon, G. *Inorg. Chem.* **1980**, *19*, 2236.
(30) Böttcher, W.; Brown, G. M.; Sutin, N. *Inorg. Chem.* **1979**, *18*, 1447.
(31) Bernhard, P.; Bürgi, H.-B.; Hauser, J.; Lehmann, H.; Ludi, A. *Inorg. Chem.* **1982**, *21*, 3936.
(32) Bard, A. J., Faulkner, L. R., Eds. *Electrochemical Methods*; John Wiley & Sons: 2nd ed., 2001.
(33) Chandler, D., Ed. *Introduction to Modern Statistical Mechanics*; Oxford University Press: Oxford, 1987.
(34) Blumberger, J.; Tateyama, Y.; Sprik, M. submitted to *Computer Phys. Comm.*
(35) Tateyama, Y.; Blumberger, J.: Sprik, M. manuscript in preparation.
(36) Yee, E. L.; Cave, R. J.; Guyer, K. L.; Tyma, P. D.; Weaver, M. J. *J. Am. Chem. Soc.* **1979**, *101*, 1131.
(37) Vuilleumier, R.; Sprik, M. *J. Chem. Phys.* **2001**, *115*, 3454.
(38) CPMD Version 3.3, Hutter, J. and Ballone, P. and Bernasconi, M. and Focher, P. and Fois, E. and Goedecker, St. and Marx, D. and Parrinello, M. and Tuckerman, M., MPI für Festkörperforschung and the IBM Zurich Research Laboratory, 1998.
(39) Troullier, N.; Martins, J. *Phys. Rev. B* **1991**, *43*, 1993.
(40) Handgraaf, J.-W.; Reek, J. N. H.; Meijer, E. J. *Organometallics* **2003**, *22*, 3150.
(41) Becke, A. D. *Phys. Rev. A* **1988**, *38*, 3098.
(42) Lee, C.; Yang, W.; Parr, R. *Phys. Rev. B* **1988**, *37*, 785.
(43) Lide, D. R., Ed. *CRC Handbook of Chemistry and Physics*; CRC Press: 75 ed., 1995.
(44) Sprik, M.; Ciccotti, G. *J. Chem. Phys.* **1998**, *109*, 7737.
(45) Andersen, H. C. *J. Comput. Phys.* **1983**, *52*, 24.